



Supplement of

Daytime-only mean data enhance understanding of land–atmosphere coupling

Zun Yin et al.

Correspondence to: Zun Yin (zyin@princeton.edu)

The copyright of individual parts of the supplement might differ from the article licence.

S1 Atmospheric advection-dominated climate regime in Sahara

Unlike most other places, the atmospheric leg (\mathcal{A}) across the Sahara region is negative (Fig. S7), suggesting a negative correlation between the sensible heat flux (H) and the pressure at the LCL (P_{lcl}). This atypical signal presents in all seasons and may be caused by a special mechanism driven by atmospheric advection. Northerly winds from the Mediterranean Sea cool and moisten the near-surface air of the Sahara region, while southerly winds warm and dry the surface (Fig. S8a). According to ERA5, the correlation between E-based daily northward wind speed ($v_{10\text{m}}$) and the 2-m air temperature ($T_{2\text{m}}$) for ten-year JJA data at a sample grid cell in the Sahara is 0.63 (Fig. S8b), which is much larger than that of the eastward wind case (0.12, not shown). On the other hand, the northerly winds show a high correlation with the 2-m absolute humidity (AH), as well (-0.67, Fig. S8b). This suggests that atmospheric advection may determine the inter-daily fluctuations of near-surface temperature and humidity rather than the sensible heat flux from the surface. One piece of evidence is that $T_{2\text{m}}$ fluctuates synchronously with H in the Sahara, with Fig. S8c showing that the auto-correlation is strongest with no time lag between variables. If the $T_{2\text{m}}$ is driven by the surface through H then the peak correlation should occur with a few hours time lag between H and $T_{2\text{m}}$, as shown for an example European grid cell in Fig. S8d.

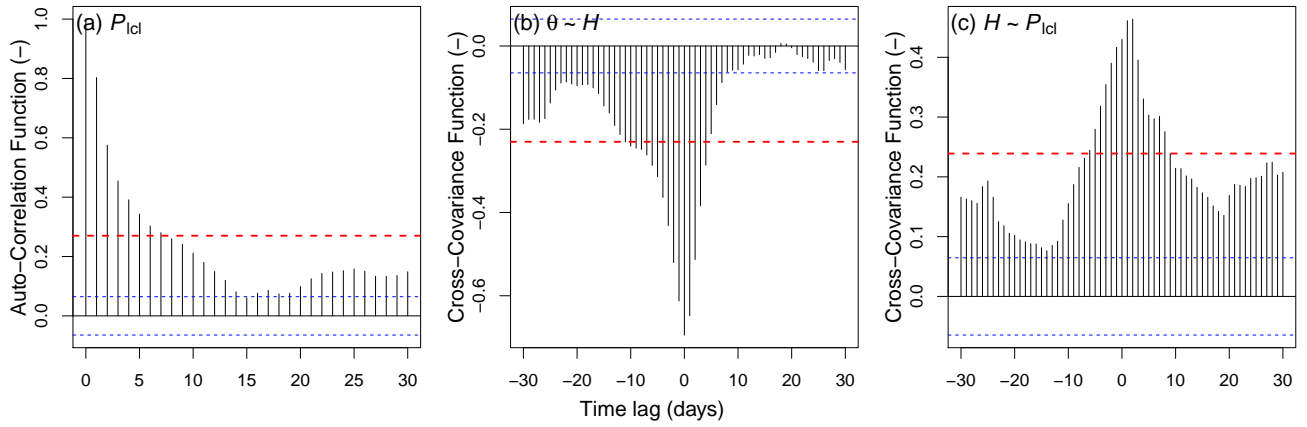


Figure S1. Examples of calculating memory indicator for the σ term and for the numerator of the ρ term ($N(\rho)$) of the two-legged metrics. (a) The entire-day-mean-based $\sigma_{P_{lcl}}$ for instance, at one grid cell we first calculate the auto-correlation function (ACF) of P_{lcl} with the maximum lag of 30 days. Then the top 25% quantile of these correlation coefficients are selected (red dashed lines indicate the threshold) and averaged as the indicator $\overline{ACF}_{>75\%}$. (b) For the paired θ and H , we calculate the cross-covariance function (CCF) with the maximum lag of ± 30 days. As the $\rho(\theta, H)$ is negative, we select the lowest 25% correlation coefficients and calculated the mean ($\overline{CCF}_{<25\%}$) as indicator. (c) Similar to (b), but selecting the top 25% correlation coefficients to calculate the indicator.

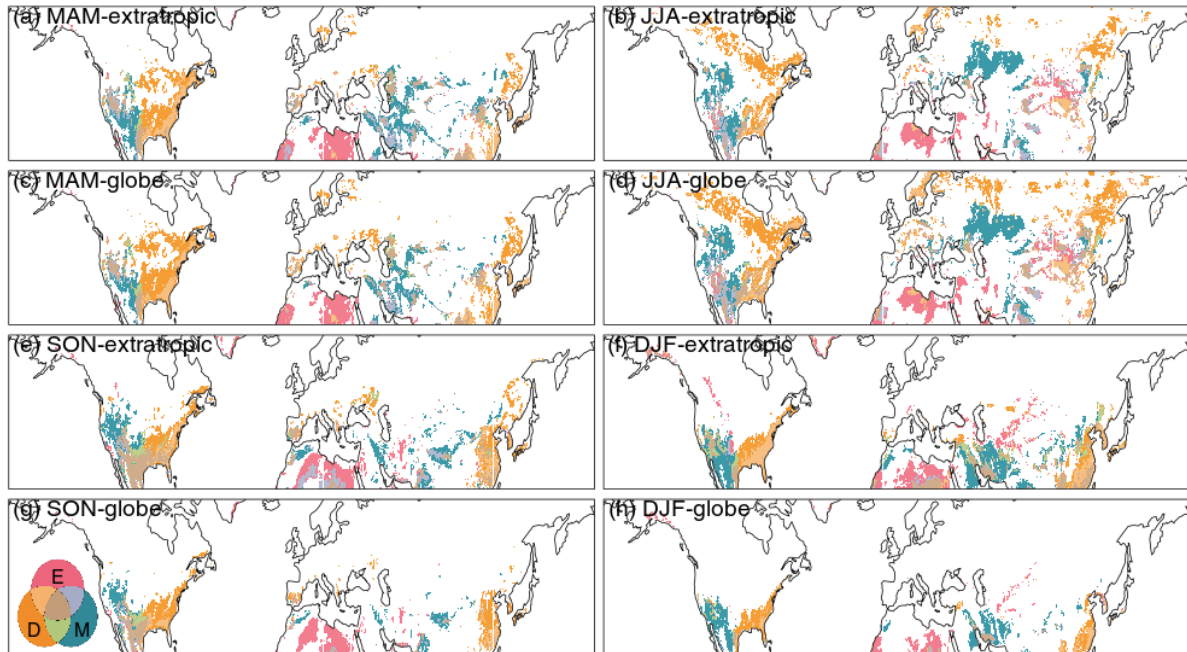


Figure S2. Spatial patterns of significant \mathcal{A}_M , \mathcal{A}_E , and \mathcal{A}_D (top 10% quantile of absolute values) of different seasons in the extratropical region of the Northern Hemisphere. Euler diagrams show the colors for specific relationships (intersections, unions, or disjoint) among \mathcal{A}_M , \mathcal{A}_E , and \mathcal{A}_D . (a), (b), (e), and (f) are screenshots from the global quantile analysis. (c), (d), (g), and (h) are based on quantile analysis of the illustrated region.

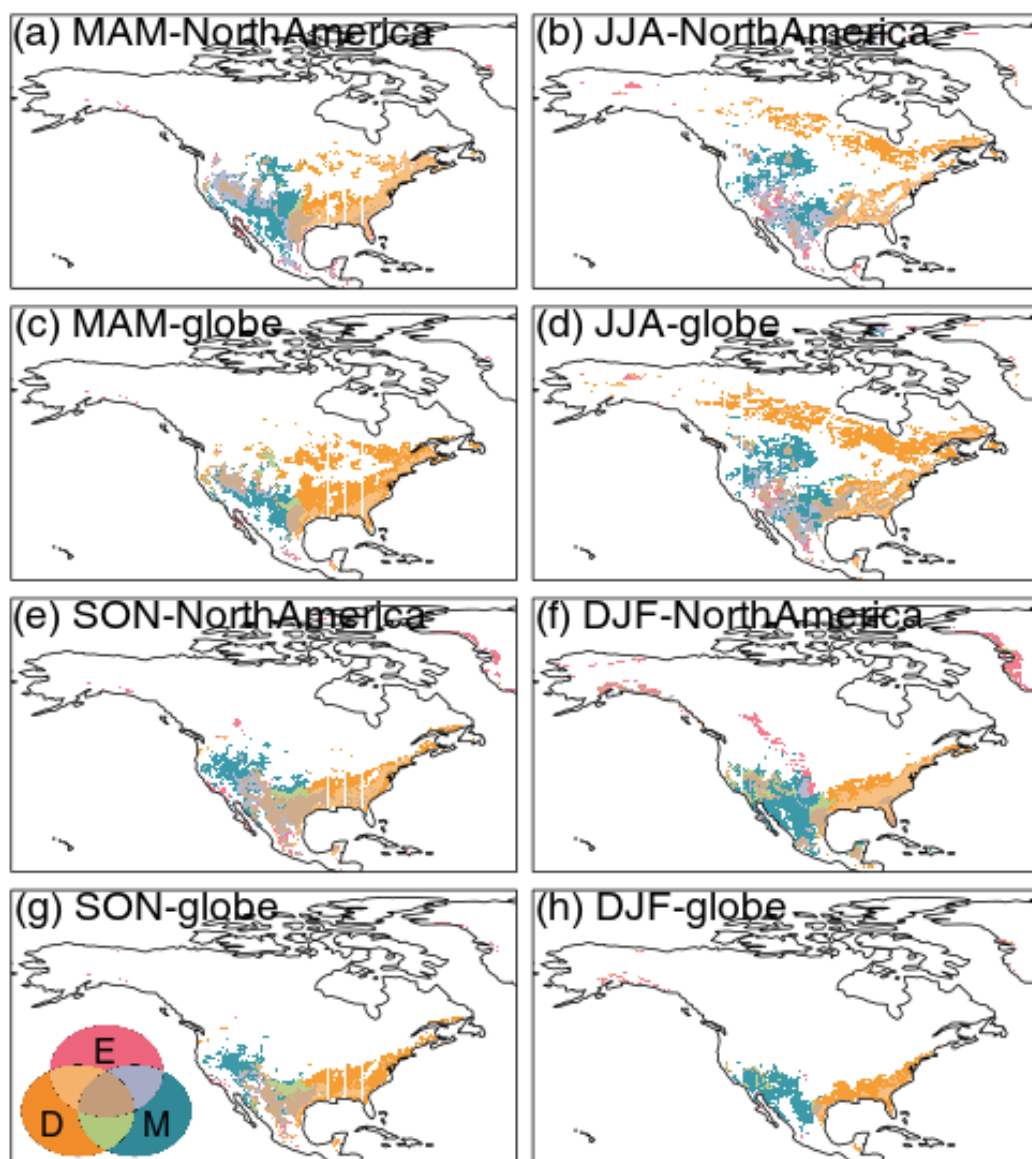


Figure S3. Spatial patterns of significant \mathcal{A}_M , \mathcal{A}_E , and \mathcal{A}_D (top 10% quantile of absolute values) of different seasons in North America. Euler diagrams show the colors for specific relationships (intersections, unions, or disjoint) among \mathcal{A}_M , \mathcal{A}_E , and \mathcal{A}_D . (a), (b), (e), and (f) are screenshots from the global quantile analysis. (c), (d), (g), and (h) are based on quantile analysis of the illustrated region.

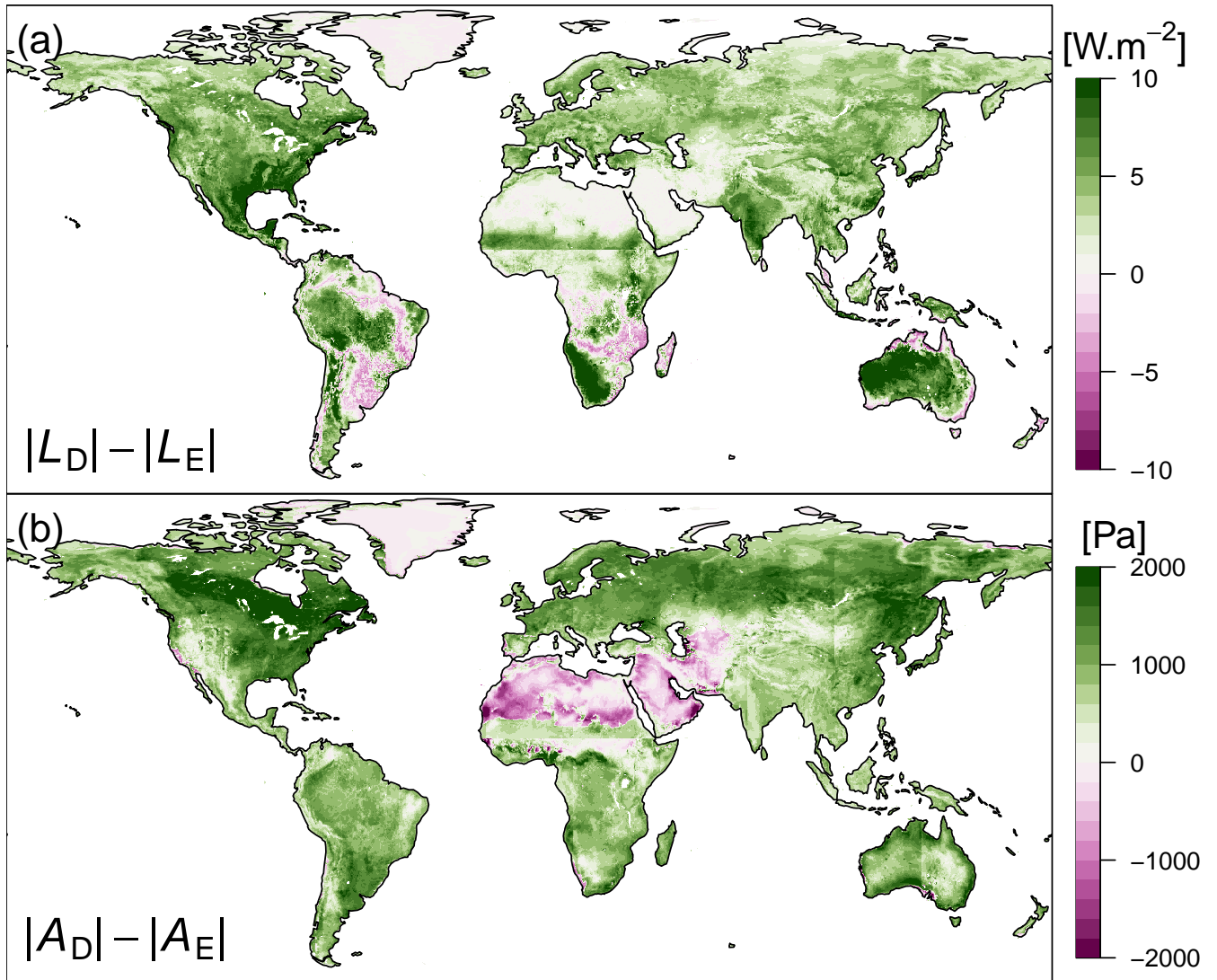


Figure S4. (a) Difference between $|L_D|$ and $|L_E|$ in summer (JJA and DJF for the Northern and Southern Hemisphere, respectively). (b) Same as (a) but for the atmospheric leg (\mathcal{A}).

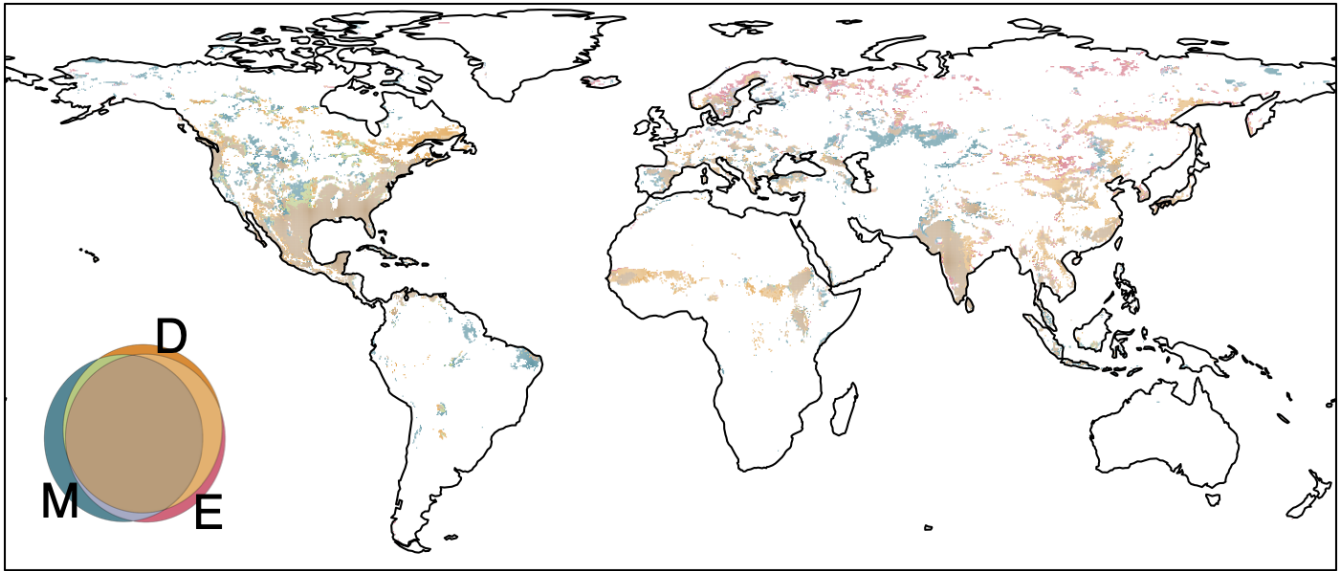


Figure S5. Spatial patterns of significant \mathcal{L}_M , \mathcal{L}_E , and \mathcal{L}_D (top 90% quantile of absolute values) in summer (JJA and DJF in the Northern and Southern Hemisphere, respectively). Euler diagrams show the colors for specific relationships (intersections, unions, or disjoint) among \mathcal{L}_M , \mathcal{L}_E , and \mathcal{L}_D , and the areas of colored patterns indicate the fractions of them as well.

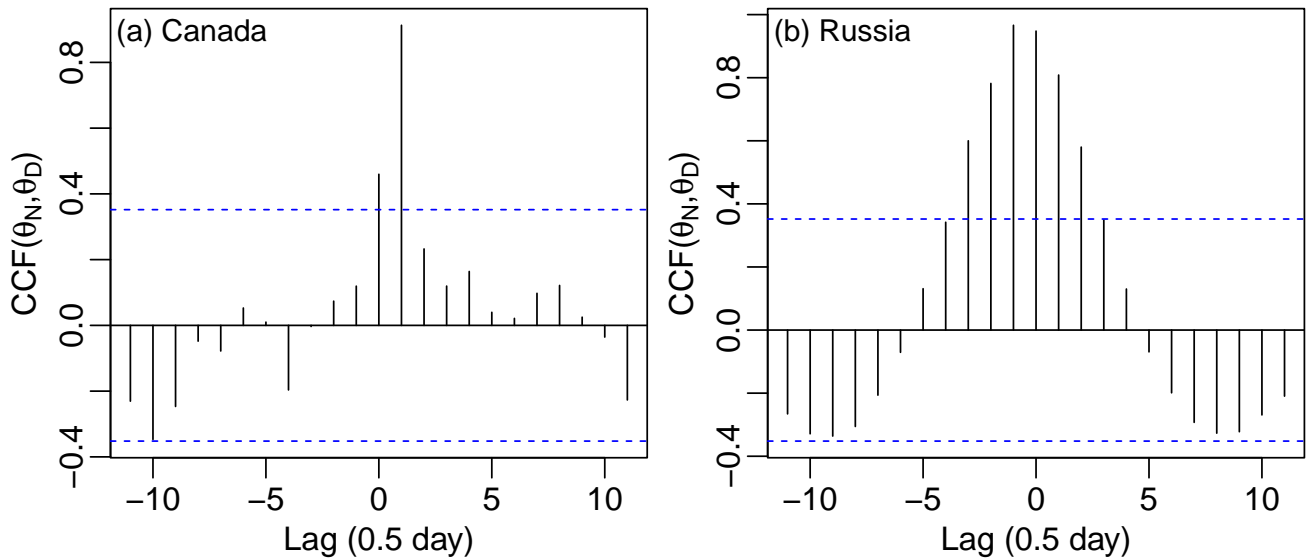


Figure S6. (a) Cross-correlation function between nighttime-only-mean (N) and daytime-only-mean (D) soil moisture (θ_N and θ_D) in a grid cell located in Canada ($[82.25^\circ\text{W}, 47.5^\circ\text{N}]$). (b) Same as (a), but the grid cell is taken as a reference in Russia ($[122.5^\circ\text{E}, 68.5^\circ\text{N}]$).

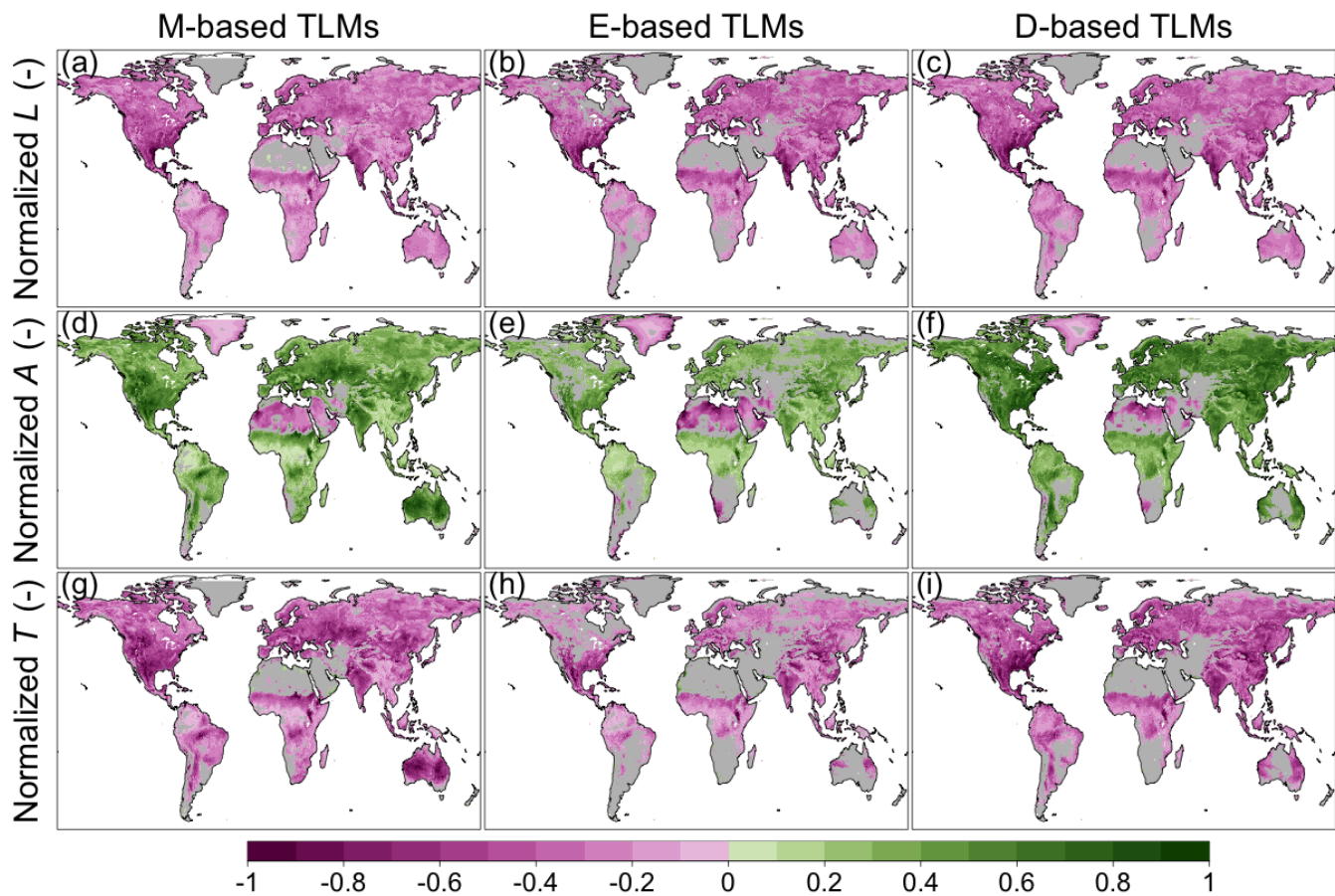


Figure S7. Maps of normalized two-legged metrics (TLMs) in JJA. Top to bottom panel: land, atmospheric, and total leg. Left to right panel: monthly-, entire-day-mean-, and daytime-only-based TLMs. To make the TLM_M , TLM_E and TLM_D comparable, we normalize specific TLM by $n_i = \min(\max(x_i/q_{99.9\%}, -1), 1)$, where n_i indicates the normalized value of x_i and the $q_{99.9\%}$ is the 99.9% quantile of $|x_i|$. Gray regions indicate associated correlation is not significant ($p \geq 0.05$)

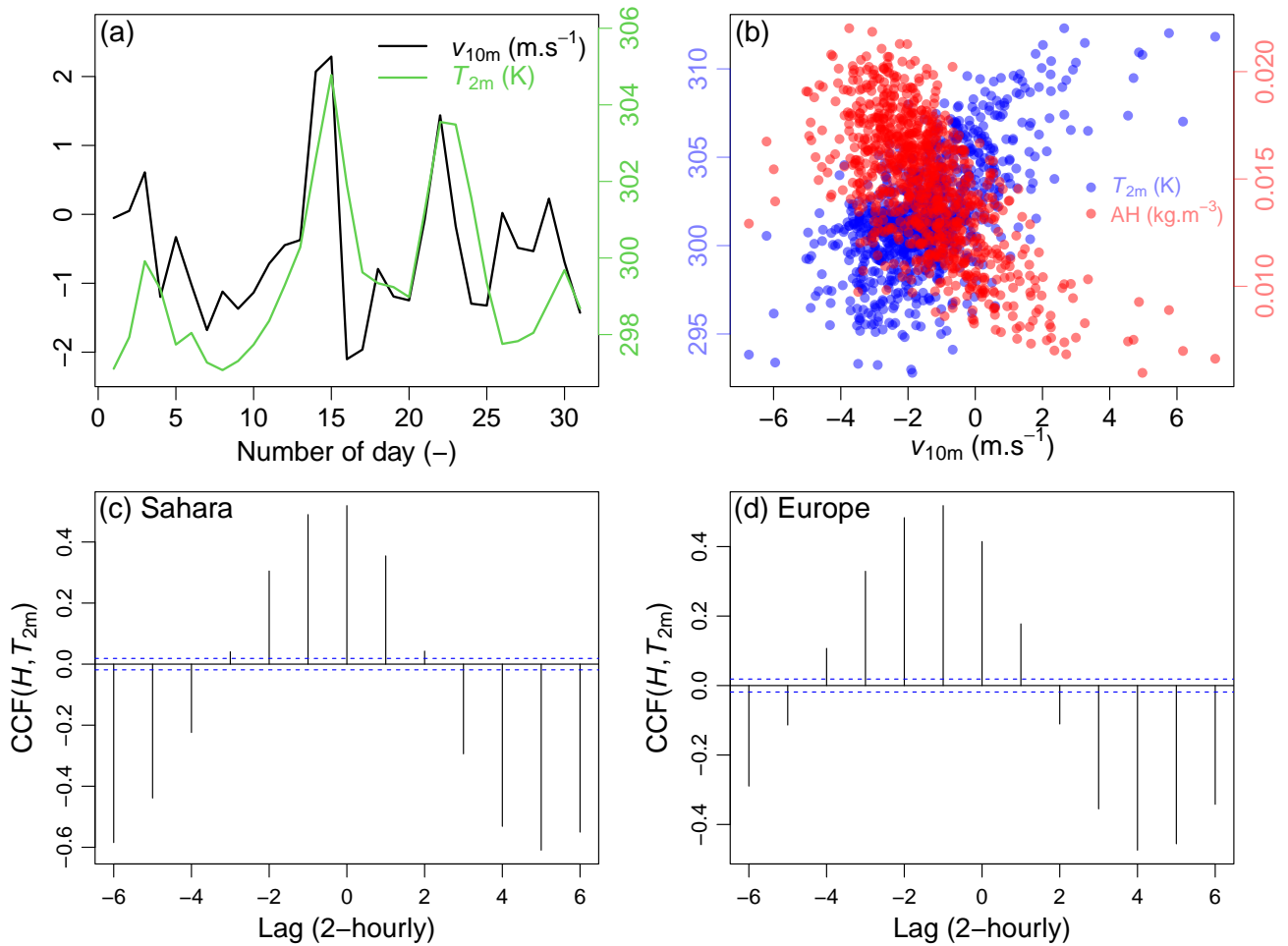


Figure S8. An example of atmospheric advection driven L-A interaction mechanism. (a) Daily 10-m northward wind speed (v_{10m}) and T_{2m} for the entire day in July 2015. (b) T_{2m} and 2m absolute humidity (AH) as a function of v_{10m} . The illustration is based on entire-day-mean daily values in JJA from 2011 to 2020. (c)–(d) Cross-covariance between two-hourly H (positive up) and T_{2m} based on two grid cells in Sahara ([12°E, 32.75°N]) and in Europe ([12°E, 47.75°N]), respectively. y -axis indicates the correlation coefficients between T_{2m} and a time-shifted H time series. The x -axis indicates the time steps of the H shifted. Negative (positive) values indicate lagged (ahead).